URA/SISA Analysis for GPS-Galileo ARAIM Integrity Support Message

Santiago Perea Díaz*, Michael Meurer*†, Markus Rippl*, and Boubeker Belabbas*
*Institute of Communications and Navigation, German Aerospace Center (DLR)
†Chair of Navigation, RWTH Aachen University, Germany
Mathieu Joerger and Boris Pervan
Illinois Institute of Technology

BIOGRAPHY

Santiago Perea Díaz obtained a Master of Science in Aerospace Engineering from University of Sevilla (Spain) in 2013. In parallel, as a double degree student, he gained his Master in Mechanical and Aerospace Engineering from Illinois Institute of Technology (IIT) in 2013. Currently he is part of the staff at the Institute of Communications and Navigation at German Aerospace Center (DLR). His research focuses on new advanced algorithms for multi-constellation Residual Autonomous Integrity Monitoring (RAIM).

Dr. Michael Meurer received the diploma in electrical engineering and the PhD degree from the University of Kaiserslautern, Germany. After graduation, he joined the Research Group for Radio Communications at the Technical University of Kaiserslautern, Germany, as a senior key researcher, where he was involved in various international and national projects in the field of communications and navigation both as project coordinator and as technical contributor. From 2003 till 2013, Dr. Meurer was active as a senior lecturer and Associate Professor (PD) at the same university. Since 2006 Dr. Meurer is with the German Aerospace Centre (DLR), Institute of Communications and Navigation, where he is the director of the Department of Navigation and of the center of excellence for satellite navigation. In addition, since 2013 he is a professor of electrical engineering and director of the Institute of Navigation at the RWTH Aachen University. His current research interests include GNSS signals, GNSS receivers, interference and spoofing mitigation and navigation for safety-critical applications.

Markus Rippl received his Diploma in Electrical Engineering and Information Technology from Technische Universitat Munchen (TUM) in 2007. Since then, he has been a research associate with the Institute of Communications and Navigation at the German Aerospace Center (DLR), in Oberpfaffenhofen near Munich. His field of work is the integrity of GNSS-based navigation using receiver-side algorithms.

Boubeker Belabbas obtained a MSc. Degree in Mechanical Engineering from ENSEM in Nancy (France) and a specialized MSc. Degree in Aerospace Mechanics from SUPAERO in Toulouse (France). He joined DLR in 2001 and developed the navigation integrity activities. He now leads the GNSS integrity team within the Department of Navigation at the Institute of Communications and Navigation. His field of competence includes GNSS with augmentations (SBAS, GBAS), Advanced Receiver Autonomous Integrity Monitoring, GNSS/INS Hybridization with integrity, and Alternative Positioning Navigation and Timing.

Dr. Mathieu Joerger obtained a Diplôme d'Ingénieur in Mechatronics from the Ecole Nationale Suprieure des Arts et Industries de Strasbourg, France, in 2002, and a M.S. and a Ph.D. in Mechanical and Aerospace Engineering from the Illinois Institute of Technology (IIT), in 2002 and 2009 respectively. He is the 2009 recipient of the Institute of Navigation (ION) Parkinson award, and the 2014 recipient of the IONs Early Achievement Award. He is currently a research assistant professor at IIT, working on multi-sensor integration, on sequential fault-detection for multi-constellation navigation systems, and on relative and differential receiver autonomous integrity monitoring (RAIM).

Dr. Boris Pervan is a Professor of Mechanical and Aerospace Engineering at IIT, where he conducts research on advanced navigation systems. Prior to joining the faculty at IIT, he was a spacecraft mission analyst at Hughes Aircraft Company (now Boeing) and a postdoctoral research associate at Stanford University. Prof. Pervan received his B.S. from the University of Notre Dame, M.S. from the California Institute of Technology, and Ph.D. from Stanford University. He is an Associate Fellow of the AIAA, a Fellow of the Institute of Navigation (ION), and Editor-in-Chief of the ION journal NAVIGATION. He was the recipient of the IIT Sigma Xi Excellence in University Research Award (2011, 2002), Ralph Barnett Mechanical and Aerospace Dept. Outstanding Teaching Award (2009, 2002), Mechanical and Aerospace Dept. Excellence in Research Award (2007), University Excellence in Teaching

Award (2005), IEEE Aerospace and Electronic Systems Society M. Barry Carlton Award (1999), RTCA William E. Jackson Award (1996), Guggenheim Fellowship (Caltech 1987), and Albert J. Zahm Prize in Aeronautics (Notre Dame 1986).

ABSTRACT

This paper presents a URA/SISA analysis to support ARAIM based on a time-dependent statistical characterization of orbit and clock errors observations. For each individual GPS and Galileo satellites, by comparing precise orbits to broadcast ephemeris data, this work computes the Signal in Space Range Error (SISRE) which needs to be overbounded by the URA/SISA value included in the ISM. Over seven years of service history data for GPS and four months for Galielo are computed in this analysis, showing that range error is manly driven by satellite's clock performance. Satellites that historically have presented well behaved σ_{SISRE} are equipped with stable clocks which display small error dispersion. A particular example is provided through GPS SVN65/PRN24 whose Cesium clock worsens satellite's performance as compared to the rest of the GPS block IIF equipped with Rubidium clocks. Time-dependent results show that orbit and clock error distributions are not zero mean on a monthly basis, although they do not exhibit a significant bias in a long-term scale. This fact might open the possibility of a short-time adaptable b_{nom} and σ_{URA} overbounding parameters contained in the ISM.

I. INTRODUCTION

Satellite navigation is undergoing a process of profound changes. The modernization of GPS with a new generation of satellites along with the development of the emerging Galileo constellation will provide new navigation signals and frequencies which will improve the performance of Advanced Receiver Autonomous Integrity Monitoring (ARAIM). Using measurement redundancy, the ARAIM airborne algorithm performs consistency checks capable of detecting and excluding ranging measurements coming from potentially faulty satellites. In GNSS Safety-of-Life (SoL) applications such as aircraft precision approach, navigation safety is guaranteed based on whether or not *integrity*, *continuity* and *accuracy* requirements are fulfilled. In order to evaluate these three performance metrics, inputs from ground monitoring stations, captured in the Integrity Support Message (ISM), are required.

The Air Navigation Service Provider (ANSP) is in charge of establishing the content of the ISM. Its dissemination depends on the ARAIM architecture, which can be either online (with an update period of about one hour) or offline (monthly updates) [1]. For both architectures, ISM contains one decisive parameter for the integrity requirement evaluation: the User Range Accuracy (URA), also called Signal in Space Accuracy (SISA). The URA/SISA is a one-sigma estimate that is used to indicate confidence in the integrity of the satellite. Physically, URA/SISA accounts for satellite orbit and clock errors caused by uncertainty in the Orbit Determination and Time Synchronization (ODTS) process, which is carried out by the Constellation Service Provider (CSP). URA/SISA is regarded as a reliability commitment from the CSP on satellite ranging measurements [2].

For GPS, previous work has shown that URA transmitted within the navigation message loosely overbounds the accuracy of the range measurements leading to an unnecessary conservatism and, therefore, loss of availability [3]. As a consequence, there is sufficient motivation for the ANSP to provide its own URA/SISA values within the ISM that ultimately lead to tighter integrity bounds. This paper proposes a statistical observation method to analyze URA/SISA based on orbit and clock a posteriori error measurements for each individual GPS and Galileo satellite.

The first part of the paper focuses on the quantitative characterization and comparison of nominal orbit and clock errors across GPS and Galileo satellites and their impact on the SISRE disregarding time dependence. The second part revisits the stationarity assumption of the error and analyzes its time-variation by breaking service history down into monthly datasets. Conclusions extracted from the results of both approaches will be included in the final section of this paper. Recommendations for the ISM dissemination and possible applications of a time-adaptable overbound will also be discussed.

II. METHODOLOGY

A. Satellite orbit and clock error

Satellite orbit and clock errors are defined as the deviations of the instantaneous satellite Antenna Phase Center (APC) and clock provided by Broadcast Ephemeris (BCE) from the Precise Reference Orbit (PRO) position and satellite clock bias. Throughout this work, the three-dimensional orbit error vector will be expressed in satellite's reference body frame Radial, Along-Track and Cross-Track (RAC) as described in figure 1.

Both BCE and PRO datasets are required in the evaluation of the orbit and clock errors. Broadcast ephemeris datasets contain the actual navigation message transmitted by each individual satellite to GNSS users. They are utilized to emulate user's calculation of satellite position and clock based on orbital parameters contained in the navigation message.

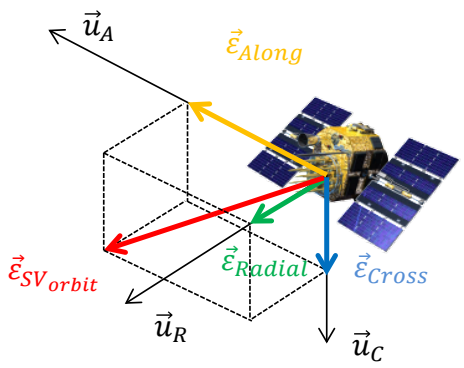

Figure 1: Satellite body frame errors

In a post-process analysis, estimated satellite positions by the users are compared to the precise reference orbit. The resulting discordance between these two inputs is the so-called orbit and clock error vector.

B. Data Source

This work utilizes BCE files supplied by the International GNSS Service (IGS) openly available through its online repository [4]. By means of a worldwide network of over 400 volunteer reference stations [5], IGS records individual satellite messages and compiles the so-called *brdc* files. Theses files collect GPS navigation data on a daily basis provided in RINEX 2 in day-of-the-year format ***brdc****ddd0.yy****n***.

In the case of Galielo, data recorded by the Muli-GNSS Experiment (MGEX) of the IGS are used as source [6]. In contrast to the previous GPS navigation files, those elaborated by MGEX network (a total of 125 Stations by August 2015 [7]) provide multi-GNSS broadcast ephemeris data for GPS, GLONASS, Galileo, Beidu, QZSS and SBAS for over 85 satellites. Multi-GNSS BCE files are provided in RINEX 3 format jointly elaborated by the Technical University of Munich (TUM) and the German Aerospace Center (DLR). They are compiled on a daily basis in the so-called *brdm* files which are openly available through its online repository [8]. Files nomenclature is again organized in day-of-the-year format ***brdm****ddd0.yy****n***.

Despite GPS BCE information is also included within *brdm* files, it is important to note that MGEX files hold a shorter service history than IGS itself. In particular, TUM/DLR Multi-GNSS ephemeris files are available since first day of the year 2013 while GPS-only BCE repository contains data from back in the 90s. Next subsection will reasonably detail the service history period under study that has been selected for each constellation.

Precise ephemeris datasets contain accurate satellite's position and clock information considered as 'truth' reference data. Among all institutions that supply precise orbit and clock data for GPS, it was decided to utilize reference files provided by the Center of Orbit Determination in Europe (CODE) located at the Astronomic Institute of the University of Bern (AIUB). GPS orbit and clock data have been extracted from the final GNSS orbits *cod* files in SP3c format accessible through its online archive [9]. Precise products computed by CODE analysis center provide daily GPS orbit and clock data with 15 minutes sampling in day-of-the-week format (***cod****wwwwd.****sp3***) and display accuracies at the 2-3 cm level [10].

For Galileo precise orbit data, Technical University of Munich products are used as reference. Galileo orbit and clock data are provided in daily ***tum****wwwwd.****sp3*** files with 5 minutes sampling interval starting on GPS week 1711. They are also publicly available in MGEX online repository [11]. Respectively, Galileo precise orbit and clock accuracies oscillates between 10 and 15 cm.

C. Nominal Performance Assumption

The URA/SISA characterization carried out in this work concentrates on satellite's nominal orbit and clock error. The evaluation of the constellation nominal performance based on service history data might be jeopardized by two types of events: satellite faults and data outliers.

According to GPS Standard Position Service Performance Standard (GPS SP SPS) [2] a satellite is considered to present a major fault if its average projected error is greater than $4.42 \cdot \sigma_{URA}$. Although satellite fault detection and characterization is an essential task to asses GNSS integrity, the identification of faulty events falls outside the scope of this study. Exhaustive and documented work has been presented in [3] where five major GPS faults were identified since 2008. The analysis in this paper has consequently suppressed the orbit and clock error samples coming from those five corresponding periods.

Service history data outliers might result in apparent satellite's faults which are only a consequence of an error in the compilation of BCE files. Along this line, previous work has exposed inconsistencies within *brdc* files which do not fully correspond to the actual message broadcast by the satellites [12]. Discrepancies mainly affected Time of Clock, Issue of Data Clock and Time of Transmission of the Message. This paper profits from the algorithm developed in the cited work which generates consistent and 'clean' broadcast ephemeris files for GPS satellites.

D. Time frame and monitored satellites

The selection of the service period under analysis and the choosing of satellites that will be included in this study

have been done with special care. Two factors are taken into account when selecting the proper data sample from all the available history data for GPS and Galileo: major updates in the Operational Control Segment (OCS) ground infrastructure and decommission of old satellites (only applicable to GPS).

In case of GPS ground facilities, the addition of eleven NGA monitor stations by the end of 2006 provided triple visibility to Orbit Determination and Time Synchronization process [13]. Respectively, a recent Galileo system upgrade occurred during February-March 2015 when a full-scale hardware and software migration was carried out along with the inclusion of three new monitoring stations. An overall 25% performance improvement in the constellation performance has been reported by the European Space Agency (ESA) [14]. As a result, using data prior to those respective events might not be representative of the current and/or future performance of the GPS and Galileo constellation.

With respect to decommissioned GPS satellites, it has been considered not to analyze orbit and clock error corresponding to satellites that were deactivated before February 2015 (end of period under study). Section IV will expose substantial differences among GPS blocks which will reinforce the idea of only analyzing currently operational satellites to assess present or future performance.

On those grounds, this paper inspects orbit and clock nominal error for GPS constellation from January 1, 2008 through February 28, 2015 and for Galileo constellation from March 1 through June 30, 2015 for the following satellites:

- **GPS Block IIA**: SVN32/PRN23, SVN26/PRN26, SVN34/PRN04 and SVN40/PRN10.
- **GPS Block IIR**: SVN43/PRN13, SVN46/PRN11, SVN51/PRN20, SVN44/PRN28, SVN41/PRN14, SVN54/PRN18, SVN56/PRN16, SVN45/PRN21, SVN47/PRN22, SVN59/PRN19, SVN60/PRN23, SVN61/PRN02, SVN53/PRN17, SVN52/PRN31, SVN58/PRN12, SVN55/PRN15, SVN57/PRN29, SVN48/PRN07 and SVN50/PRN05.
- **GPS Block IIR**: SVN65/PRN25, SVN63/PRN01, SVN65/PRN24, SVN66/PRN27, SVN64/PRN30, SVN67/PRN06, SVN68/PRN09 and SVN69/PRN03.
- **Galileo**: GSAT0101/E11, GSAT0102/E12 and GSAT0103/E19

This work has ensured that no changes has occurred for any of the SVN/PRN couples during the course of this analysis. PRN change information can be found in the Notice Advisory to Navstar Users (NANU) files provided by the US Coast Guards Navigation Center [15].

E. Two Approaches

Throughout this work, the statistical study of satellite orbit and clock nominal error will follow two different procedures attending to its stationarity. First approach merges all the healthy service history data available for each satellite disregarding variations over time. A quantitative characterization of the four error components (Radial, Along-Track,Cross-Track and Clock) and their impact on SISRE is archived with this approach. Results will be included in Section IV.

The second approach revisits the prior stationarity assumption. By breaking GPS service history down into monthly datesets (although other intervals could be selected) this work analyzes variations in error distribution's bias and standard deviation over time. This methodology will be further described in Section V.

III. SISRE DEFINITION

Every user located at a point within the satellite's coverage footprint possesses a different Line-of-Sight (LOS) unitary vector $\vec{e}$ and will consequently experience a different Instantaneous User Range Error (IURE). The transcription from satellite orbit error to pseurodange error is a simple matter of vector projection (see figure 2). According to GPS SPS SP, Signal-in-Space Range Error can be defined as the average contribution over all the IURE values of users located within the visibility cone of the satellite [2].

In this work a slightly different interpretation of SISRE is used. For any given satellite orbit error vector, we define SISRE as the worst user projection (wup) within satellite's footprint (instead of averaging). In other words, it accounts for the maximum (or minimum) IURE. The determination of the wup is originally tree-dimensional but it can be reduced to a 2D problem in the 'worst case plane' ($\mathcal{W}$).

Plane $\mathcal{W}$ is defined by the satellite's orbit error vector $\vec{\varepsilon}_{sv,orb}$ and radial unit vector $\vec{u}_R$ described in figure 1. Note that any other plane in $\mathcal{R}^3$ than the 'worst case plane' will contained a projection of the original orbit error with a consequent reduction of its norm. Let $\vec{u}_V$ be an orthogonal unit vector to $\vec{u}_R$ also contained in $\mathcal{W}$ so that $\{\vec{u}_R, \vec{u}_V\}$ is an orthonormal basis of $\mathcal{W}$. As shown in figure 2, $\mathcal{W}$-cone section defines an arc of a circle on Earth's surface where the worst user location (wul) should be contained.

The projection of the orbit error vector into the candidate worst user location's LOS can be parametrized with θ. Each θ_i defines a survey $\vec{e}_{s,i}$ into which $\vec{\varepsilon}_{sv,orb}$ is projected

$$IURE_{orb,i} = \vec{\varepsilon}^{T}_{sv,orb} \cdot \vec{e}_{s,i} \tag{1}$$

where

$$\vec{e}_{s,i} = cos\theta_i \vec{u}_R + sin\theta_i \vec{u}_V \quad \text{and} \quad \theta_i = [-\varphi, \varphi]\,. \tag{2}$$

As represented in figure 2 the semiangle of the visibility cone φ is unique for each constellation and depends on the semi-major axis of the satellite orbit: $\varphi_{GPS} = 13.9°$ and $\varphi_{GAL} = 12.4°$. Satellite clock error ε_{clock} equally influences all user range measurements and its effect shall be subtracted in the final IURE computation as follows

$$IURE_i = IURE_{orb,i} - \varepsilon_{clock}. \tag{3}$$

Finally, SISRE evaluation selects the worst case from the $IURE_i$ set,

$$SISRE = \max(|IURE_i|) \cdot \text{sgn}(IURE_i). \tag{4}$$

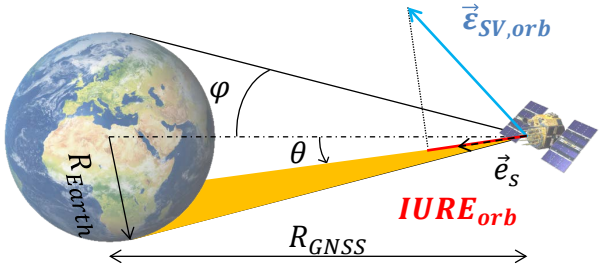

Figure 2: Worst user projection search

The main difference between this expression and the one obtained by averaging (GPS SPS SP) is the preservation of the actual sign of IURE in SISRE. However SISRE distribution is bimodal as a consequence of the non-zero definition (there is always a non-zero IURE for each given orbit error). This will be relevant in the characterization of SISRE dependence on each individual orbit and clock error in the following Section IV.

IV. ORBIT AND CLOCK ERROR: DISTRIBUTION AND CORRELATION

This section addresses the first of the two approaches previously mentioned. For both GPS and Galileo constellations we pursue a statistical characterization of Radial, Along-Track, Cross-Track and Clock error with a particular focus on their distribution biases and dispersions. Table 3 at the end of this paper gathers the corresponding parameters for each individual satellite. However, given the large number of satellites under analysis, results is this section are clustered by block type and constellation in order to bring to light the diversity among them.

Statistical results are presented in three different formats: Relative Frequency Histograms, Cumulative Distribution Functions (CDF) and parameters tables. A peculiar type of CDF has been utilized in this section; the so-called folded Cumulative Distribution Function or *mountain plot* [16]. This technique folds the second half of the CDF plot by inverting the y scale for values of $x \in [m, \infty)$, being m the median of the distribution. Contrary to traditional CDF curves, mountain plots ease the visualization of the tails of both sides of the distribution as well as the evaluation of the distribution symmetry.

Correlation between SISRE and individual orbit and clock error is evaluated through scatter plots for each constellation and block type. Each plot includes the value of the covariance between Radial, Along-Track, Cross-Track, Clock error and SISRE along with the correlation coefficient defined as $\rho_{x,y} = \sigma_{x,y}/(\sigma_x \cdot \sigma_y)$ in [17]. (Note that $\sigma_{x,y}$ values are expressed in $m \cdot m$).

A. GPS Constellation

A total of 31 GPS satellites have been analyzed from 1/1/2008 to 2/28/2015 with a result of 6,171,331 orbit and clock nominal error samples. Figures 3 and 4 respectively correspond to relative frequency histogram and folded CDF plots merging all GPS samples. In addition table 1 provides a breakdown analysis of the individual distribution biases and standard deviations.

SISRE bimodality becomes clear in figure 3 where the probability decreases around the zero error value. It can also been observed that satellite's along-track direction presents the largest error magnitude and dispersion. This trend repeats all over the analyzed satellites being an effect of the poor observability in the ODTS process in that direction. Cross-track is secondly ranked in error magnitude and dispersion. This error presents a peculiar half sidereal day periodicity which can be explained by satellite's orbital equations of motion. Radial direction typically exhibits the smallest orbit error and dispersion.

In order to compare the differences among blocks presented in table 1, it is important to remind that precise orbit and clock files accuracy stands between 2-3 cm for GPS. On a long term basis and disregarding time-dependence, orbit and clock error distributions are nearly zero mean. That is reflected in both figure 10 and table 1 where the mean values of the distributions do not exceed accuracy's order of magnitude. Along-track error is an exception to the previous statement which can be explained by the visibility issue already mentioned. It can be observed in table 1 that μ_{SISRE} acquires a large value for GPS Block IIF satellites. In essence, the mean value of SISRE does not have a significant interpretation given the bimodality of the distribution. The fact that μ_{SISRE} presents a larger

value for Block IIF than for the rest of GPS satellites only reflects the asymmetry of the distribution.

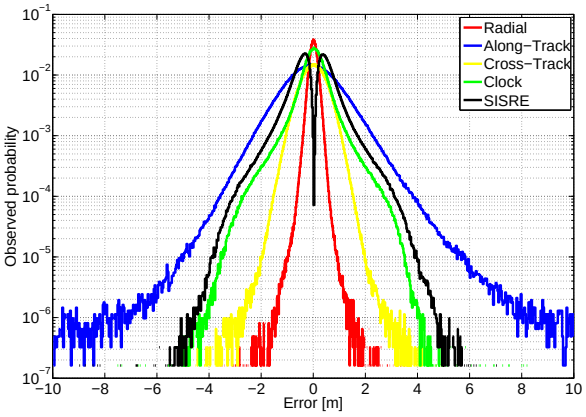

Figure 3: GPS orbit and clock error Relative Frequency Histogram from 1/1/2008 to 2/28/2015

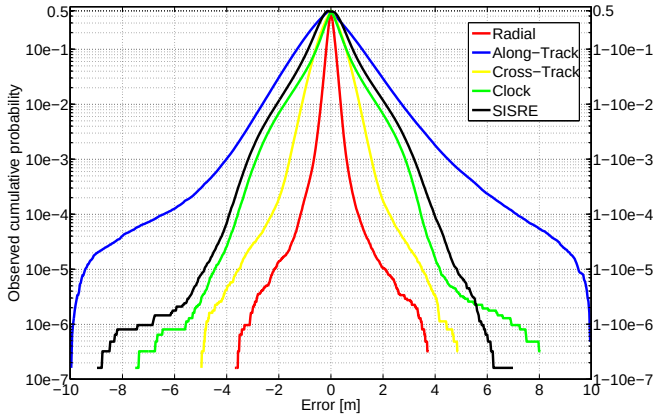

Figure 4: GPS orbit and clock error folded CDF from 1/1/2008 to 2/28/2015

Another relevant remark is the similarity of the standard deviation values between blocks. Radial, along-track and cross-track errors show a resembling performance for Block IIA and Block IIR with a marginal improvement for Block IIF. However σ_{clk} certainly exhibits an enormous contrast among blocks which is automatically translated into SISRE standard deviation. Table 1 shows that $\sigma_{clk}^{IIA} \gg \sigma_{clk}^{IIR} \gg \sigma_{clk}^{IIF}$ and $\sigma_{SISRE}^{IIA} \gg \sigma_{SISRE}^{IIR} \gg \sigma_{SISRE}^{IIF}$ consequently manifesting that SISRE performance is driven by satellite clock error.

Attending to on-board clock type considerations, SVN65 / PRN24 data has been excluded from block IIF characterization. While the rest of Block IIF satellites operate with Rubidium clocks, this satellite currently works with a backup Cesium clock. Figure 5 shows that SVN65/PRN24 performance is comparable to 1996-launched Block IIA satellite SVN40/PRN10 which is also equipped with a Cesium clock; it results in a deterioration of the whole block IIF performance. Extracting data from table 3, while distribution σ_{clk} stands well below 40 cm for block IIF rubidium clock satellites, SVN65 / PRN24 presents a σ_{clk} of 109 cm, in the same order of SVN40 / PRN10 with a σ_{clk} of 122 cm.

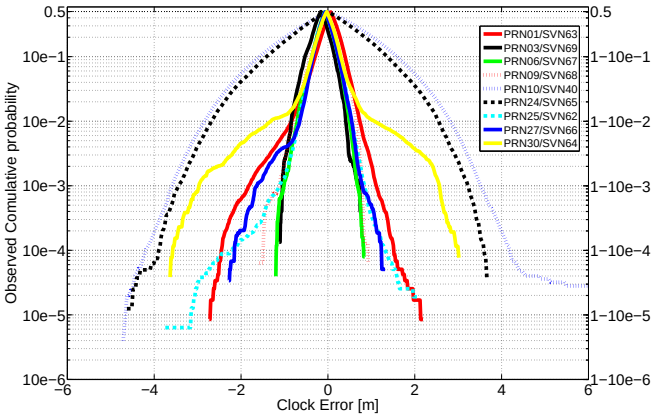

Figure 5: GPS Block IIF clock comparison - Folded CDF

A second aspect regarding clock error distribution can be observed in figure 5; block IIF satellite clock errors present asymmetric distributions. This is specially pronounced for those satellites with small clock dispersion like SVN66 / PRN 27 ($\sigma_{clk} = 25cm$) and SNV62 / PRN25 ($\sigma_{clk} = 26cm$). The causes of this asymmetry are still unknown to the authors and future versions of this work will deepen in the this issue.

Correlation between SISRE and the individual orbit and clock errors is studied through scatter plots included in figures 6, 7 and 8 for blocks IIA, IIR and IIF respectively. The dominance of the clock error in SISRE over the rest is a common factor in all analyzed satellites. However it cedes influence in favor of radial error as clock performance enhances from block IIA to block IIF with correlation coefficients of $\rho_{rad,sisre}^{IIF} = 0.537$ and $\rho_{clk,sisre}^{IIF} = -0.768$. Scatter plots also reflect SISRE bimodality. Lines $y = \pm sin(\varphi_{GPS})x$, set by satellite's visibility cone, delimit two regions of the data cloud for along-track and cross-track errors. Geometrically, these lines demarcate the maximum projection of the along-track and cross-track component of the orbit error into user's LOS.

Table 1: Error distribution parameters by blocks (values in cm)

Constellation type	Radial		Along-Track		Cross-Track		Clock		SISRE		Number of Samples
	μ	σ	μ	σ	μ	σ	μ	σ	μ	σ	
GPS Block IIA	-4.4	19.5	9.8	120.1	-0.3	43.0	-0.1	84.7	-4.5	106.3	988,342
Block IIR	0.4	13.26	-7.6	101.4	0.0	48.0	2.3	50.8	-3.0	70.7	4,693,693
GPS Block IIF*	6.1	19.0	-18.8	103.6	-0.1	37.9	-2.9	28.7	13.2	55.1	408,986
All GPS	0.1	15.3	-5.7	105.2	0.0	46.5	1.4	57.5	-2.0	77.8	6,171,331
All Galileo	8.6	43.7	-101.5	176.2	-1.0	90.0	0.7	72.8	-14.0	106.7	98,035

* Excluding SVN65/PRN24 (80310 healthy samples)

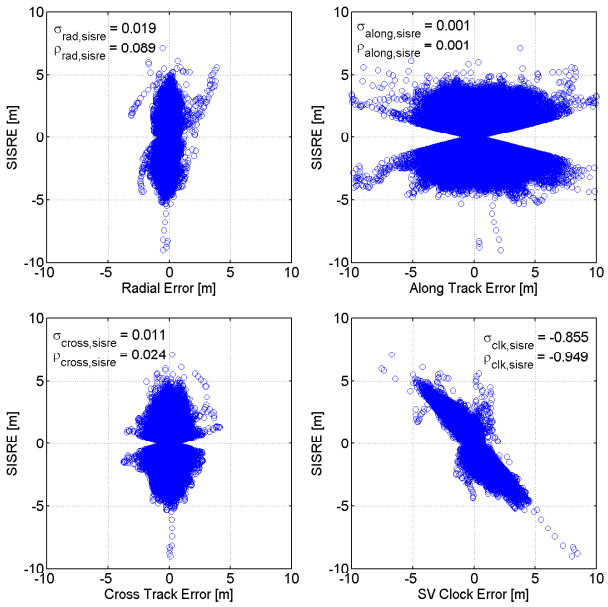

Figure 6: Scatter plot Orbit and Clock error vs SISRE for GPS Block IIA from 1/1/2008 to 2/28/2015 ($\sigma_{x,y}$ in $m \cdot m$)

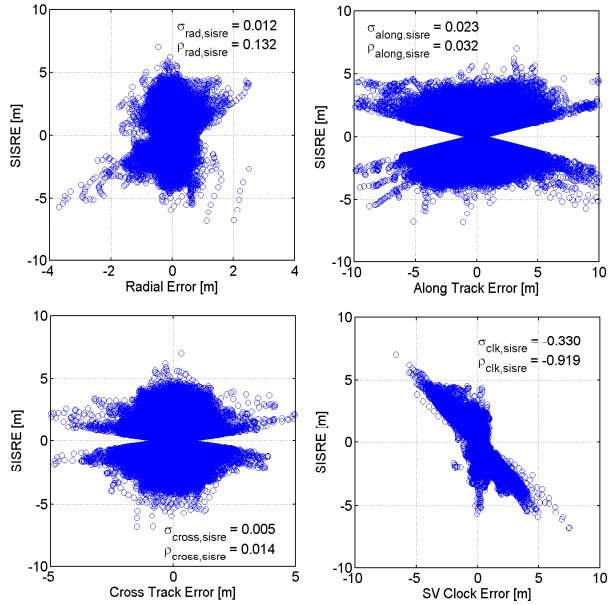

Figure 7: Scatter plot Orbit and Clock error vs SISRE for GPS Block IIR from 1/1/2008 to 2/28/2015 ($\sigma_{x,y}$ in $m \cdot m$)

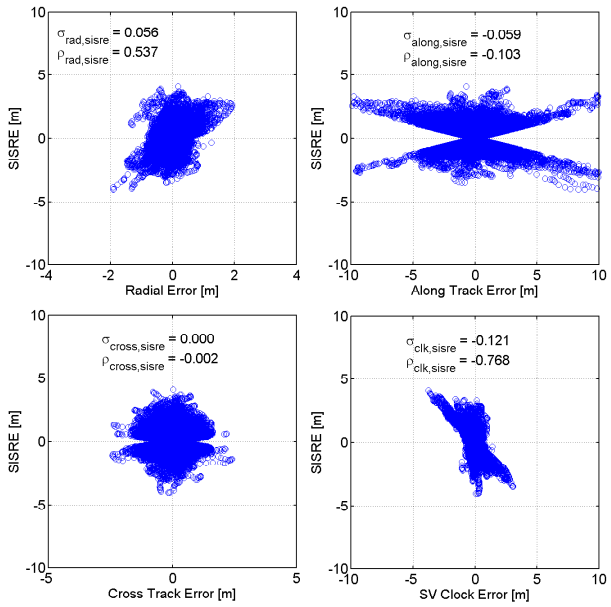

Figure 8: Scatter plot Orbit and Clock error vs SISRE for GPS Block IIF from 1/1/2008 to 2/28/2015 ($\sigma_{x,y}$ in $m \cdot m$)

B. Galileo Constellation

The fact that Galileo has not still reached its Full Operational Capability (FOC) makes the characterization of the orbit and clock errors less solid than for GPS, not because of the suitability of the methodology here applied but because of the full deployment of the ground control segment. Given the implantation phase that Galileo is undergoing, it is reasonable to accept that ODTS process' current performance is not fully representative of the final Galileo FOC integrity commitment.

Along this line, several outliers have been found during the evaluation of the errors. In order to preliminary asses Galileo's SISRE performance, this work excludes those outliers attending to a threshold criteria. For each individual error an ample limit value has been set; a radial threshold of 4 m, a threshold of 10 m for both along-track and cross-track and a clock threshold of 6 m. A total of 1,325 samples have been excluded representing the 1.33% of the 99,360 original samples; out of those, 1,253 exclusions have been executed by the clock threshold criteria.

Results illustrated in relative frequency histogram and folded CDF (figures 9 and 10) exhibit similar qualitative (not quantitative) error distributions to GPS. Given that accuracy for reference orbit stands between 10-15 cm, Galileo orbit and clock errors can be considered as nearly-zero mean during the four months period under study. Same mentioned trend in the orbit error magnitude can be observed for Galileo where along-track error is the largest, followed by cross-track and radial error. As occurred in GPS case, along-track error presents a substantial bias (ODTS visibility issue). Attending to design specifications [18], Galileo satellites are equipped with high-grade Rubidium clocks and its navigation message has a 10 minutes update interval (rather than 2 hours). Therefore, $\sigma_{clk} = 78cm$ and $\sigma_{SISRE} = 106.7cm$ for Galileo included in table 1 might be a pessimistic guess of the future FOC performance of the constellation.

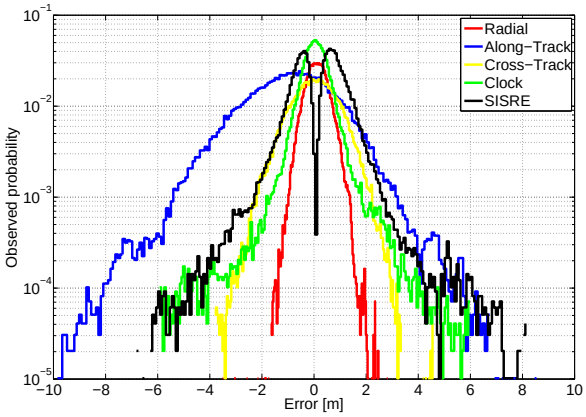

Figure 9: Galileo orbit and clock error Relative Frequency Histogram from 3/6/2015 to 6/30/2015

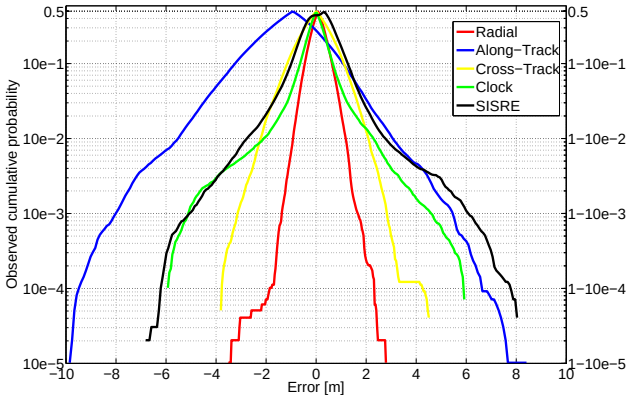

Figure 10: Galileo orbit and clock error folded CDF from 3/6/2015 to 6/30/2015

Regarding correlation between errors, scatter plots in figure 11 show the prevalence of clock over orbit error in SISRE. As it ocurred in GPS block IIF (figure 8), a future enhancement on satellite clock performance might concede larger dominance in favor of radial error.

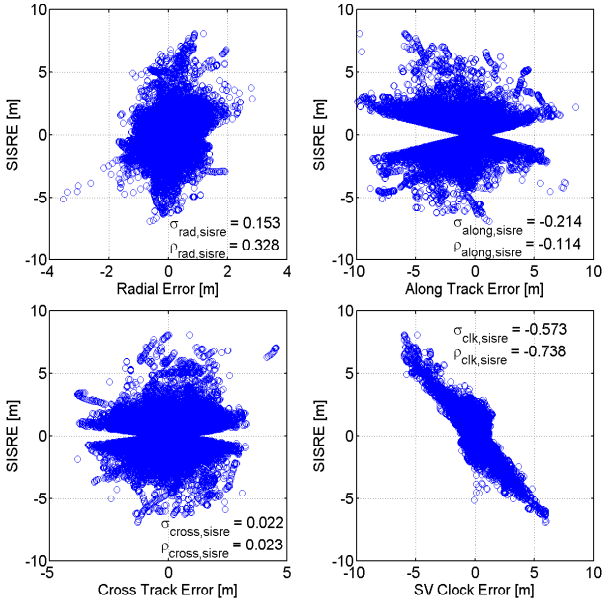

Figure 11: Scatter plot Orbit and Clock error vs SISRE for Galileo from 3/6/2015 to 6/30/2015 ($\sigma_{x,y}$ in $m \cdot m$)

V. ORBIT AND CLOCK ERROR: STATIONARITY ANALYSIS

This section addresses the second approach in which the stationarity assumption is revisited from an integrity perspective. The characterization of satellite orbit and clock error by merging all the service history data in a single distribution (as done in the previous section) does not provide sufficient information about the performance of the error in a short-time scale. In particular, this work addresses the question of how long do we need to monitor a satellite to confidently characterize its nominal performance. To find an answer, satellite's service history is divided in monthly datasets starting from January 2008 (or usable date) to February 2015. Unfortunately the fact that Galileo is still under IOV phase and that last ODTS update occurred in the first quarter of 2015 limits the implementation of this breakdown methodology for the European constellation (only three full months of data). Future revisions of this work (when more service history data become available) will deepen into Galileo orbit and clock error's stationarity.

For each GPS satellite, final table 3 compares both methodologies: stationarity versus time-dependence. Each row shows maximum values of mean and standard deviation reached in a monthly error analysis (μ_{mx} , σ_{mx}) and compares them to values obtained by merging all available service history data (μ_{all} , σ_{all}). A common aspect observed in all satellites is the transition period during its accommodation in the constellation. In the first 1-1.5 months of operation, satellite orbit and clock errors are not representative of the nominal operation than they do

show after this insertion period. It has been consequently accounted in the computation of μ_{mx} and σ_{mx} by disregarding the two first datasets in the search of the maximum.

More detailed information about error time-dependence is provided in table 2 which uses block IIF GPS satellite SVN67 / PRN06 as a breakdown example. Each row of table 2 shows the monthly mean and standard deviation of satellite orbit and clock error distributions including datasets from June 10, 2014 to February 28, 2015. Furthermore, three-dimensional *waterfall diagrams* concatenate each folded CDF for every individual month. Figures 12 and 13 respectively display those diagrams for clock error and SISRE distributions where the already defined 'accommodation period' is visible through the tails of the distributions during the first two months. However, once this transition is over, clock and radial error biases reach values up to 13-15 cm. Along-track error presents the largest bias variations over months (observability from ODTS) while cross-track error possesses a stable nearly zero mean behavior over time.

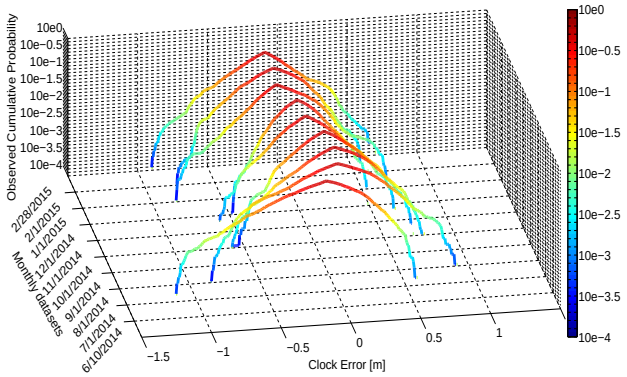

Figure 12: GPS SVN67/PRN06 Clock Error Folded CDF waterfall monthly diagram from 6/10/2014 to 2/28/2015

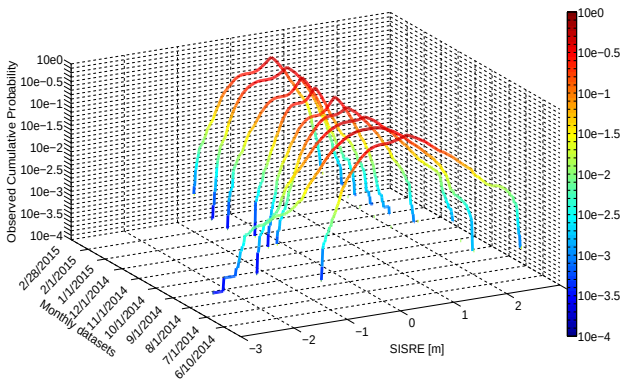

Figure 13: GPS SVN67/PRN06 SISRE Folded CDF waterfall monthly diagram from 6/10/2014 to 2/28/2015

Given these results, it can be stated that satellite orbit and clock errors distributions are neither zero mean nor constant on a short-time basis. Regarding standard deviations, they tend to suffer smaller relative variations. However, it is difficult to assess that driving parameters like σ_{rad} and σ_{clk} remain constant with less than 8-10 cm variations over time and consequently it is hard to assess that σ_{SISRE} does. Given the non-stationarity of the error, characterizing a satellite performance by looking at short periods of time (months) is not feasible and hence a time-adaptable overbound might be more efficient.

VI. CONCLUSIONS

The analysis of the satellite orbit and clock error described throughout this paper can be used to elaborate a series of recommendations for σ_{URA} dissemination within the ISM. Results have shown that SISRE does not perform similarly for all the satellites, even within same block type. Consequently, ISM shall account for this diversity of satellite's performances by including individual σ_{URA} values which allow users to perform different overbounds to each ranging measurement. This work has also shown that SISRE's behavior is mainly driven by satellite clock error, finding enormous differences between satellites equipped with Rubidium and Cesium clocks.

Error stationarity evaluation has exposed the so-called 'accommodation period' that satellites undergo right after their insertion in the constellation. Approximately during the first 40-50 days of operation, satellites experience unusually large SISRE values which are not representative of the actual performance after this tunning process. In order to achieve an efficient overbound σ_{URA} computation shall account for those events.

Regarding error biases, results demonstrate that satellite orbit and clock errors can be considered nearly zero mean within accuracy level 2-3 cm for GPS and 10-15cm for Galileo in a long term observation period. However, time-dependence analysis has shown that error means are not only non-zero in short-time periods but also time-variant on a monthly basis. In the same sense, it is difficult to assess that σ_{SISRE} remains constant with less than 8-10 cm variations over time. Those statements might open the possibility of performing a time-adaptive overbound within ISM. It may also include a trade-off methodology where σ_{URA} takes a less conservative value in favor of accounting for orbit and clock biases in b_{nom}. Consolidation of this concept is left for future versions of this work.

Table 2: PRN06 monthly error distribution parameters (values in cm)

Dataset period	Radial		Along-Track		Cross-Track		Clock		SISRE	
	μ	σ	μ	σ	μ	σ	μ	σ	μ	σ
Jun 2014	6.7	37.0	-31.4	122.7	-31.3	67.4	-16.3	31.7	34.4	76.6
Jul 2014	4.4	41.5	-34.2	137.4	-11.9	35.3	-0.8	30.2	6.1	-78.0
Aug 2014	12.3	36.8	-48.1	139.3	-1.8	47.2	4.1	24.2	11.4	71.1
Sep 2014	13.7	22.8	63.6	89.8	-3.8	30.5	2.0	20.1	18.7	51.63
Oct 2014	11.5	12.3	69.7	75.9	3.1	37.9	-5.6	19.5	29.1	40.7
Nov 2014	6.7	11.2	-26.0	84.2	5.4	42.4	-6.4	16.1	23.2	37.1
Dec 2014	5.3	13.1	-0.9	78.4	-3.7	53.7	-13.7	21.6	28.7	42.5
Jan 2015	5.9	19.6	20.8	87.7	0.3	63.8	-13.7	22.6	27.2	54.4
Feb 2015	6.2	23.8	18.7	92.9	0.7	55.9	-15.5	22.9	31.7	50.2
All	8.1	26.3	-26.2	107.8	-2.5	49.8	-6.9	24.5	22.9	57.7

ACKNOWLEDGMENTS

The authors would like to deeply thank Dr. Oliver Montrenbruck from the German Space Operation Center (GSOC) for his inestimable contribution with the error evaluation software. In addition, we thank Dr. Todd Walter from Stanford University's GPS Lab for providing clean GPS navigation files.

REFERENCES

[1] Working Group C, ARAIM Technical Subgroup, EU-US Cooperation in Satellite Navigation. Milestone 2 Report. February, 2015.

[2] *Global Positioning System Standard Positioning Service Performance Standard*, U.S. Department of Defence, 4th Ed. September 2008, pp A-22, Std.

[3] T. Walter and J. Blanch, "Charactrization of GPS Clock and Ephemeris Errors to support ARAIM," in *Pacific PNT Meeting, Honolulu, HI*, April 20-23.

[4] International GNSS Service Repository, ftp://cddis.gsfc.nasa.gov/gps/data/daily/.

[5] International GNSS Service Station List, https://igscb.jpl.nasa.gov/network/list.html.

[6] O. Montenbruck, P. Steigenberger, R. Khachikyan, G. Weber, R. B. Langley, L. Mervart, and U. Hugentolber, "IGS-MGEX Preparing the Ground for Multi-Constellation GNSS Science," *Inside GNSS*, pp. 42–49, January/February 2014.

[7] Multi-GNSS Experiment Station List, http://www.igs.org/network?network=multi-GNSS.

[8] Multi-GNSS Experiment Repository, ftp://cddis.gsfc.nasa.gov/gnss/data/campaign/mgex.

[9] CODE Repository, "ftp://ftp.unibe.ch/aiub/code."

[10] O. Montenbruck, P. Steigenberger, and A. Hauschild, "Broadcast versus precise ephemeris: a multi-gnss perspective," *GPS Solutions*, June 2014.

[11] Technical University of Munich / MGEX Repository, ftp://cddis.gsfc.nasa.gov/pub/gps.

[12] L. Heng, G. Gao, T. Walter, and P. Enge, "GPS Signal-in-Space Integrity Performance Evolution in the Last Decade," *IEEE Transactions on Aerospace and Electronic Systems*, vol. 48, no. 4, pp. 2932–2946, October 2012.

[13] B. Wiley, D. Craig, D. Manning, J. Novak, R. Taylor, and L. Wiengarth, "NGA's Role in GPS," in *International Technical Meeting of the Satellite Division of the Institute of Navigation, Fort Worth, TX*, Sept. 26-29 2006.

[14] European Space Agency, "Galileo System Update and Back to work," http://www.esa.int, April 2015.

[15] United States Coast Guards Navigation Center, http://www.navcen.uscg.gov/?pageName=gpsNanuInfo.

[16] K. L. Monti, "Folded Empirical Distribution Function Curves-Mountain Plots," *The American Statistician*, vol. 49, no. 4, pp. 342–345, November 1995.

[17] D. C. Montgomery and G. C. Runger, *Applied Statistics and Probability for Engineers*, 3rd ed. John Wiley & Sons, Sept 2002.

[18] *Galileo Signal in Space Interface Control Document*, European Global Navigation Satellite Systems Agency Std.

Table 3: Satellite orbit and clock error distribution parameters : monthly breakdown vs. full service history

PRN SVN	Radial				Along-Track				Cross-Track				Clock				SISRE	
	μ_{mx}	μ_{all}	σ_{mx}	σ_{all}	μ_{mx}	μ_{all}	σ_{mx}	σ_{all}	μ_{mx}	μ_{all}	σ_{mx}	σ_{all}	μ_{mx}	μ_{all}	σ_{mx}	σ_{all}	σ_{mx}	σ_{all}
BLOCK IIA																		
32/23	-13.4	-4.1	30.7	21.6	127.2	9.3	170.4	115.6	8.8	0.8	105.7	50.2	36.8	9.0	78.3	65.4	104.0	84.8
26/26	-21.7	-4.9	45.5	18.0	165.5	16.6	187.8	124.5	-5.8	-1.0	68.5	39.4	-37.8	-0.1	144.8	42.5	163.7	84.9
04/39	-17.3	-4.7	28.7	16.6	174.2	16.5	186.4	116.8	4.6	-0.3	64.0	38.9	20.4	-4.5	116.5	75.9	135.4	97.5
10/40	-14.3	-4.0	32.3	21.5	-124.9	-3.1	204.3	122.0	-6.0	-0.5	67.0	42.6	76.7	1.6	141.8	122.0	167.4	145.1
BLOCK IIR																		
13/43	5.3	-0.2	19.1	11.8	-66.2	-15.6	144.3	91.0	-11.3	0.0	70.0	47.5	22.4	-2.2	73.4	42.2	93.0	62.3
11/46	17.4	7.9	22.8	14.6	117.4	-7.3	154.4	107.1	-18.3	-0.8	65.4	40.9	34.7	8.8	83.0	60.3	105.3	80.4
20/51	5.8	-0.2	22.9	10.8	-90.4	58.3	154.1	96.4	-14.2	-0.6	72.9	47.2	-18.3	-3.0	65.5	31.2	78.8	53.4
28/44	18.5	10.3	17.4	12.8	-91.5	-26.3	126.7	99.6	10.1	0.5	59.6	41.3	38.0	16.4	127.2	105.5	149.9	124.8
14/41	-10.5	-0.2	19.5	12.0	121.9	-7.5	123.1	98.4	-10.8	-0.1	67.7	43.6	20.5	1.8	63.7	37.7	78.9	58.4
18/54	7.8	1.5	17.6	12.2	-99.6	2.7	128.2	95.7	12.1	0.6	82.9	47.2	-15.1	-0.8	82.2	34.8	100.0	55.3
16/56	-9.5	-5.6	16.5	11.6	-84.2	-3.5	138.3	94.7	-7.4	0.4	81.3	48.7	-26.7	8.9	36.7	28.3	66.3	49.4
21/45	12.5	2.8	27.5	12.7	-110.8	-8.5	146.8	103.1	14.7	0.4	84.4	51.2	23.3	5.9	75.4	33.9	94.2	57.0
22/47	-13.8	-9.8	15.4	12.0	67.8	-5.3	126.4	100.8	-15.0	-0.1	103.5	56.0	38.0	7.2	94.8	79.3	112.6	98.0
19/59	-6.5	-2.2	15.4	10.3	-81.7	-25.0	143.9	92.7	-15.4	-0.3	103.6	58.3	-28.6	-13.9	42.1	32.9	70.8	54.6
23/60	-7.1	-2.9	14.6	11.1	-83.6	-6.1	112.3	90.7	-7.5	0.2	75.3	43.0	-16.5	12.4	40.1	28.0	62.5	49.3
02/61	9.4	4.1	16.6	10.4	66.4	1.9	131.4	86.8	15.3	0.2	69.7	49.6	-64.2	6.7	73.0	34.3	89.0	53.9
17/53	23.9	5.7	20.8	12.9	136.9	1.5	205.5	119.9	14.7	0.5	110.9	59.2	25.9	7.8	86.7	67.1	131.6	91.0
31/52	9.3	1.9	17.4	12.5	137.9	8.7	121.8	104.6	6.2	0.3	63.1	41.8	-27.4	-2.7	80.7	57.6	101.8	78.1
12/58	12.1	5.9	21.2	13.2	-121.7	-6.4	147.0	108.2	-9.1	-0.2	73.0	39.0	31.8	11.5	58.9	29.5	81.7	52.0
15/55	-7.1	-3.1	18.2	11.9	105.6	-6.7	132.8	101.6	-10.5	-0.6	76.1	43.9	26.7	9.3	35.3	27.4	61.1	48.9
29/57	-6.7	-2.0	22.7	14.3	-92.5	9.3	158.6	127.1	-12.8	-0.1	98.5	51.2	43.0	12.2	83.7	61.8	106.0	85.3
07/48	-12.6	-3.5	21.5	13.6	-121.9	-12.1	154.0	96.1	6.1	0.7	84.3	55.6	-24.6	-9.0	53.3	42.1	84.7	64.4
05/50	-11.0	-2.9	18.8	13.1	-90.9	-6.9	139.7	90.4	-14.7	-0.4	60.8	36.4	-16.6	-0.7	35.3	29.8	67.7	49.6
BLOCK IIF																		
25/62	11.1	5.3	30.5	17.5	-96.8	-12.0	144.7	93.5	4.4	-0.4	53.9	35.9	-21.8	-6.2	38.1	25.5	61.3	50.0
01/63	11.8	5.7	25.9	16.2	-114.9	-39.8	136.2	101.7	-8.6	0.4	61.0	40.9	25.6	5.0	45.7	30.0	80.7	56.7
24/65*	13.1	6.9	33.0	24.7	51.7	-19.4	165.0	112.0	-2.0	-0.7	53.7	38.5	13.6	-2.0	126.1	108.8	147.0	131.6
27/66	16.0	7.4	29.6	19.4	-90.6	-6.5	128.2	113.1	3.7	0.3	37.5	29.8	17.7	-5.9	38.1	24.9	63.4	53.2
30/64	11.2	6.8	27.9	20.4	54.4	11.4	114.0	86.4	-1.7	-0.4	50.8	39.7	6.4	-3.3	45.0	39.1	58.2	58.98
06/67	13.7	8.1	36.8	26.3	-69.7	-26.2	139.8	107.8	5.4	-2.5	63.8	49.8	-15.5	-6.9	24.2	24.5	71.1	57.7
09/68	9.4	6.3	42.6	27.7	-30.0	0.2	172.7	118.0	-2.6	-2.8	33.9	32.0	8.6	0.3	38.4	31.1	88.8	63.0
03/69	-	10.9	-	27.8	-	-46.1	-	172.6	-	8.0	-	40.9	-	-17.1	-	26.5	-	66.4
GALILEO																		
E11	-	6.5	-	45.7	-	-74.0	-	169.4	-	-1.7	-	78.1	-	-4.6	-	64.1	-	92.6
E12	-	6.9	-	41.4	-	-97.4	-	156.4	-	-3.2	-	101.6	-	-17.5	-	66.8	-	101.1
E19	-	12.5	-	43.6	-	-133.1	-	195.5	-	1.9	-	88.7	-	-10.9	-	83.0	-	118.2

* Operating Cs clock

Each row shows maximum values (in *cm*) of mean and standard deviation reached in a monthly error analysis (μ_{mx} , σ_{mx}) and compares them to values obtained by merging all available service history data (μ_{all} , σ_{all}). First two datasets corresponding to *accomodation period* have been excluded from the monthly computation. In case of non-applicability, '-' is represented.